Electric Field Evaluation around Slender Conductors by Collocation Boundary Element Method

Chijie Zhuang, *Member, IEEE,* Yong Zhang, and Rong Zeng, *Senior Member, IEEE*

***Abstract*—Evaluation of the electric field at the surface of a conductor, which is well described by the Poisson equation, is of great importance on many occasions in power systems. This paper proposes a collocation boundary element method where the unknown surface charge density function is assumed to be either azimuth independent or dependent. Detailed formula, including the quadrature rules and how to accelerate the computation when the target point lies far away from the integral element, are proposed. Numerical examples are shown to confirm the convergence of the method, and manifest the great advantage for the evaluation of the electric field around slender conductors.**

***Index Terms*—electric field, slender conductor, collocation boundary element method**

I. Introduction

EVALUATION of electric fields at conductor surfaces is important on many occasions in power systems. For example, when evaluating the lightning shielding failure of transmission lines, it is the surface electric field of lines that influences the inception of the streamer and then upward leader [1], [2], [3]; When predicting the corona performance as well as the acoustic noise and radio interference of a power line, the surface electric field is used as a practical criterion [4]. Therefore, the surface electric field evaluation continuously draws great attention.

Typically, the frequency of the voltage and current in power systems are relative low. The power frequency is only 50 or 60 Hz, and the frequency of lightning and most switching impulses in power systems (except VFTO) is typically well below 1 MHz or even lower. So in many cases, it is reasonable to assume that the conductors in power systems are in the electrostatic states, therefore, the electric field and potential has the relation of $\vec{E} = -\nabla u$.

To evaluate the surface electric field, the charge simulation method (CSM) has been widely used in such simulations due to its simplicity and efficiency [5]. However, the type and location of the charges, and check points are set empirically, which is not trivial for many cases; in addition, the simulation charge in CSM is usually placed away from the conductor surface, while physically, the charges shall distribute at the conductor surface. It is natural to apply a method like boundary element method (BEM) [6], in which the surface charge densities can be used as the unknowns, to obtain the electric field.

Chijie Zhuang and Rong Zeng are with the Department of Electrical Engineering, Tsinghua University, Beijing 100084, China.

Yong Zhang is with Center for Applied Mathematics, Tianjin University, China.

Manuscript received April 19, 2005; revised August 26, 2015.

BEM has been widely used in science and engineering, such as fluid mechanics, acoustics, electromagnetic, and fracture mechanics [7], [8], [9]. It attempts to use the assigned boundary conditions to fit boundary values rather than values throughout the computation domain which is defined by a partial differential equation. It generally has less degrees of freedom than FEM because it only discretizes the boundary of the computation domain. It is efficient when the surface to volume ratio is small, which is the case for slender conductors in power systems; and is suitable for unbounded exterior problems.

In this paper, considering the fact that the radius of a power conductor is much smaller compared with its length, we propose a collocation boundary element method to solve the surface charge density along the curved cylindrical elements, and then calculate the electric field. Considering the surface charge density depends also on the azimuth, we develop the BEM by assuming the charge densities depend on the axis variables, or both the axis and azimuth variables. Details on quadrature for both singular and regular integrals with asymptotic expansions are presented. Finally, the convergence of the method is numerically verified, and some examples are given.

II. Numerical methods

For simplicity, we shall focus on one-wire case, extension to multi-wire cases is straightforward. Considering a horizontal transmission wire as a cylinder of length $2L_0$ and radius R_0, we set the cylindrical axis as x-axis and the vertical direction as z-axis, the cylinder is then parameterized as

$$\Omega_c = \{\mathbf{x} \big| |x| \le L_0, (y,z) = r(\cos\theta, \sin\theta), r \le R_0, \theta \in [0, 2\pi)\}.$$

The cylinder surface is denoted by Σ and is composed of lateral surface Σ_{L} and base surface Σ_{B}. We shall denote points in $\mathbb{R}^3$ by bold letters throughout this article.

A. Exterior Poisson equation and the integral formulation

The electric potential $u(\mathbf{x})$ satisfies an exterior Poisson equation:

$$\begin{cases} -\nabla^2 u = \rho(\mathbf{x}), & \mathbf{x} \in \Omega := \mathbb{R}^3 \setminus \Omega_c \\ u \ = g(\mathbf{x}), & \mathbf{x} \in \Sigma, \end{cases} \tag{2.1}$$

subjecting to $\lim_{|\mathbf{x}|\to\infty} u(\mathbf{x}) = 0$ at the far field. Here, $\rho(\mathbf{x})$ is the space charge and $g(\mathbf{x})$ is a prescribed potential. To solve (2.1), we first homogenize it by subtracting $u_1(\mathbf{x}) = \int_{\mathbb{R}^3} G(\mathbf{x}-\mathbf{y})\rho(\mathbf{y})\,\mathbf{dy}$ where $G(\mathbf{x}) := 1/(4\pi|\mathbf{x}|)$ is the standard Green's function. Usually $\rho(\mathbf{x})$ is highly localized, and the

evaluation of $u_1(\mathbf{x})$ does not cost too many efforts. The residual potential $u_2 = u - u_1$ satisfies the Laplace equation and can be expressed as a first kind integral:

$$u_2(\mathbf{x}) = \int_\Sigma G(\mathbf{x}-\mathbf{y})\,\sigma(\mathbf{y})\,\mathrm{d}S\mathbf{y}, \forall\, \mathbf{x} \in \Sigma, \tag{2.2}$$

where $\sigma(\mathbf{y})$ is the unknown surface charge density. Once $\sigma(\mathbf{y})$ is known, we have $u(\mathbf{x}) = (u_1 + u_2)(\mathbf{x})$ for $\mathbf{x} \in \mathbb{R}^3$, and the electric field can be obtained as

$$\begin{aligned}\vec{E}(\mathbf{x}) &= -\nabla u \\ &= -\int_{\mathbb{R}^3} (\nabla_{\mathbf{x}} G)(\mathbf{x}-\mathbf{y})\rho(\mathbf{y})\mathrm{d}\mathbf{y} - \int_\Sigma (\nabla_{\mathbf{x}} G)(\mathbf{x}-\mathbf{y})\sigma(\mathbf{y})\mathrm{d}S\mathbf{y}.\end{aligned} \tag{2.3}$$

In cases where the ground plane is considered, the above integral needs minor modifications by including the image density via a modified Green's function, and we omit details here for brevity.

Generally speaking, there does not exist analytic solutions, therefore we have to resort to numerical solutions. Here we apply the collocation boundary element method, i.e., to solve σ in (2.2) numerically by setting collocation points $\mathbf{x}_i$ at the surface and solve the corresponding linear system.

B. Collocation boundary element method

The boundary element method has been successfully developed during the last few decades. Many different versions have been proposed, and here we choose the collocation BEM (CBEM) mainly for its simplicity. To start with, we first discretize the lateral surface and the base surface with cylindrical elements and ring elements, respectively.

To be precise, for the lateral surface, the x-axis interval $[-L_0, L_0]$ is discretized by $\{x_j\}_{j=1}^{N_x}$ with $N_x \in \mathbb{N}$, then the j-th cylindrical element is defined as $e_j := \{\mathbf{x} | x_j \le x \le x_{j+1}, (y,z) = R_0(\cos\theta, \sin\theta), \theta \in [0, 2\pi)\}$. For the base surface, we discretize the radius first as $\{r_k\}_{k=1}^{N_r}, N_r \in \mathbb{N}$, and define the k-th ring element as $e_k = \{\mathbf{x} | x = \pm L_0, (y,z) = r\,(\cos\theta, \sin\theta), r_k \le r \le r_{k+1}\}$. Note that both $\{x_j\}$ and $\{r_k\}$ can be either uniform or adaptive. Denote the partition of Σ by Σ_h, which is composed of all the cylindrical elements e_j and ring elements e_k.

We assume that the density function $\sigma(\mathbf{x})$ belongs to a piece-wise continuous space V, i.e.,

$$V = \{f(\mathbf{x}) :\ f(\mathbf{x})\big|_{\Sigma_B}, f(\mathbf{x})\big|_{\Sigma_L} \text{ are continuous}\}.$$

In addition, we note that $\sigma(\mathbf{x})$ is not necessarily continuous on the whole surface Σ. The numerical solution σ_h, an approximation of $\sigma(\mathbf{x})$, lies in space V_h defined as follows

$$\begin{aligned}V_h = \{f_h(\mathbf{x}) :\ & f_h\big|_{e_j} = f_h(x,\theta) \text{ is linear in } x, \text{ periodic in } \theta, \\ & f_h|_{e_k} = f_h(r) \text{ is linear in radial variable } r\}.\end{aligned} \tag{2.4}$$

To be precise, we need to refine the cylindrical element. Given e_j, we use uniform grid in the azimuth direction as $\theta_m = 2\pi m/M$, $M \in \mathbb{N}$ and enforce the periodic condition, i.e., $f_h(x,0) = f_h(x,2\pi)$. Then we have $e_j = \cup_{m=1}^M e_j^m$ with $e_j^m := \{\mathbf{x} | x_j \le x \le x_j + 1, (y,z) = r_0(\cos\theta, \sin\theta), \theta_m \le \theta \le \theta_{m+1}\}$.

A simpler V_h was used in [10] where σ_h is assumed to depend on only the x-variable over the cylindrical element. This simple method is referred to as *reduced-basis* method hereafter. However, recent studies have revealed some weak θ-dependence of the electric field distribution near the surface. Therefore, besides the reduced-basis method, we shall adopt V_h to explore the θ-dependence and refer it to *full-basis* method hereafter.

The discrete unknowns are set on the vertexes of each element, denoted by $\{\mathbf{x}_i\}_{i=1}^N$, which include all vertexes of the finest element e_j^m and $(\pm L_0, 0, r_k)^T$ of each ring element e_k. Collocation points are chosen the same as source points. To find $\sigma_h \in V_h$ such that (2.2) holds at $\mathbf{x}_i$, we have

$$u_2(\mathbf{x}_i) = \int_{\Sigma_h} G(\mathbf{x}-\mathbf{y})\sigma_h(\mathbf{y})\mathrm{d}S\mathbf{y}, \quad \mathbf{x}_i, i = 1\ldots, N. \tag{2.5}$$

Written in matrix form, the above equation reads as follows

$$A\,\sigma_h = u_{2,h}, \quad \sigma_h, u_{2,h} \in \mathbb{R}^{N\times 1}, \tag{2.6}$$

where $A = (a_{ij}) \in \mathbb{R}^{N\times N}$ is the coefficient matrix, $\sigma_h, u_{2,h}$ are the unknown densities and the potential at the collocation points respectively. The matrix entry a_{ij} is generated from a surface integral over either a cylindrical or ring element.

It is worth mentioning that Eq. (2.5) and (2.6) works for both single and multiple line cases; and can be used to evaluate the field around slender conductors depending on the required accuracy, especially for the straight metal wires. However, for curved or twisted wires, the discretization of the wire should be sufficient fine, and the azimuth dependent *full basis* method is better.

As the linear system is usually not too large, we can solve it with direct method. The formation of the matrix A requires $O(N^2)$ operations and it involves two kinds of surface integrals, i.e., an integral over a ring element at the base surface and an integral on a cylindrical element on the lateral surface. As is common, the singular or nearly-singular surface integral requires a careful treatment in order to guarantee necessary accuracy, while for the regular integral, Gaussian quadrature is readily applied and the computing efficiency is always of great concern. In this paper, the slender wires have a very small radius to length ratio, which makes it possible to speed up the regular integral computation using asymptotic analysis.

C. Stable and efficient quadrature for surface integrals

A stable and efficient quadrature is of great importance. The surface integral $I(\mathbf{x}_i) = \int_{\mathcal{E}} G(\mathbf{x}_i - \mathbf{y})\sigma_h(\mathbf{y})\mathrm{d}S\mathbf{y}$ is singular when $\mathbf{x}_i$ sits on the element $\mathcal{E}$, and is regular otherwise. Quadrature for singular integral requires a specific treatment in order to guarantee accuracy, while the efficiency is more important for regular integrals as most of required integrals are regular integrals.

For simplicity, we shall present here the strategy for *reduced-basis* method where the density σ_h is assumed to be dependent only on the x variable over the cylindrical element. As the ratio of the radius to length is very small, and the contribution from the side surface is minor, we shall focus on

integrals over lateral cylindrical elements. The methodology can also be applied to the ring element integral (those on the base surface) and *full-basis* method, we omit the adaptions for brevity.

Consider one cylindrical element of radius r_0,

$$\mathcal{E} = \{\mathbf{x}\big| x \in [x_1, x_2], (y,z) = r_0(\cos\theta, \sin\theta), \theta \in [0, 2\pi)\}.$$

The potential generated by $\sigma_h(\mathbf{x}) := f(x) = f_1 \frac{(x_2-x)}{x_2-x_1} + f_2 \frac{(x-x_1)}{x_2-x_1}$ over $\mathcal{E}$ at $\mathbf{x} = (x_0, 0, d_0)^T$ is given below

$$I = \frac{r_0}{4\pi} \int_{x_1}^{x_2} \mathrm{d}x \int_0^{2\pi} \mathrm{d}\theta \ \frac{f(x)}{\sqrt{(x-x_0)^2 + r_0^2 + d_0^2 - 2r_0 d_0 \sin\theta}}. \quad (2.7)$$

The integrand is singular when $x_0 = x_1$ or x_2 and $d_0 = r_0$, and is regular otherwise. For the singular integral, take $x_0 = x_1$ for example, (2.7) is simplified as follows

$$\begin{aligned} I &= \frac{r_0}{4\pi} \int_0^{\Delta x} \mathrm{d}x \int_0^{2\pi} \mathrm{d}\theta \ \frac{f(x+x_1)}{\sqrt{x^2 + 2r_0^2(1-\sin\theta)}} \\ &= \frac{2r_0}{4\pi} \int_{-1}^{1} \mathrm{d}t \int_0^{\Delta x} \mathrm{d}x \ \frac{f(x+x_1)}{\sqrt{x^2 + 2r_0^2(1-t)}\sqrt{1-t^2}} \\ &:= \frac{r_0}{2\pi}(f_1 I_1 + \frac{f_2 - f_1}{\Delta x} I_2), \end{aligned} \quad (2.8)$$

where

$$I_1 = \int_{-1}^{1} \frac{dt}{\sqrt{1-t^2}} \int_0^{\Delta x} \frac{dx}{\sqrt{x^2 + 2r_0^2(1-t)}}, \quad (2.9)$$

$$I_2 = \int_{-1}^{1} \frac{dt}{\sqrt{1-t^2}} \int_0^{\Delta x} \frac{xdx}{\sqrt{x^2 + 2r_0^2(1-t)}}. \quad (2.10)$$

The second identity holds by a change of variable $t = \sin\theta$ over the interval $\theta \in [-\pi/2, \pi/2]$. To compute I_1 and I_2, we first integrate the inner integral analytically, and the resulting integrand, function of t, is regular. The remaining 1-D integral can be computed with Gaussian quadrature after filtering its singular part. Take I_2 for example.

$$\begin{aligned} I_2 &= \int_{-1}^{1} \frac{\sqrt{(\Delta x)^2 + 2r_0^2(1-t)}}{\sqrt{1-t^2}} \mathrm{d}t - \int_{-1}^{1} \frac{\sqrt{2} r_0}{\sqrt{1+t}} \mathrm{d}t \\ &:= \int_{-1}^{1} \left(g_1(t) + g_2(t) + r_2(t)\right) \mathrm{d}t - 4r_0, \end{aligned} \quad (2.11)$$

where

$$g_1(t) = \frac{\Delta x}{\sqrt{2}} \frac{1}{\sqrt{1-t}}, \ g_2(t) = \frac{1}{\sqrt{2}} \frac{1}{\sqrt{1+t}} \sqrt{(\Delta x)^2 + 4r_0^2},$$

and $r_2(t) = \sqrt{(\Delta x)^2 + 2r_0^2(1-t)}/\sqrt{1-t^2} - g_1(t) - g_2(t)$ is regular. The singular components are integrated exact, i.e., $\int_{-1}^{1} g_1(t)\mathrm{d}t = 2\Delta x$, $\int_{-1}^{1} g_2(t)\mathrm{d}t = 2\sqrt{(\Delta x)^2 + 4r_0^2}$, and the remaining integral $\int_{-1}^{1} r_2(t)\mathrm{d}t$ is approximated by Gaussian quadrature. Following this way, the double integral finally comes down to a standard 1-D regular integration.

For regular integrals, one can first integrate with respect to x, then apply Gaussian quadrature to the resulting regular 1-D integrals. Fortunately, the integration can be accelerated by exploring the small radius property. When the collocation point $\mathbf{x}_i$ lies far away from the cylindrical element, the integrand can be approximated by polynomials via Taylor's expansion, then the resulting polynomials are separable and can be integrated exact. Take the case where $r_0 \ll d_0$, which is very common in multi-wire cases, for example, we first approximate the inverse of the distance function as follows

$$\begin{aligned} & \left[(x-x_0)^2 + d_0^2 + r_0^2 - 2r_0 d_0 \sin\theta\right]^{-\frac{1}{2}} \\ = \ & \left[(x-x_0)^2 + d_0^2\right]^{-\frac{1}{2}} \left[1 + \frac{r_0^2 - 2r_0 d_0 \sin\theta}{(x-x_0)^2 + d_0^2}\right]^{-\frac{1}{2}} \\ \approx \ & \sum_{p=0}^{P} C_p \left(\frac{r_0^2 - 2r_0 d_0 \sin\theta}{(x-x_0)^2 + d_0^2}\right)^p \left((x-x_0)^2 + d_0^2\right)^{-\frac{1}{2}} \\ = \ & \frac{1}{d_0} \sum_{p=0}^{P} C_p \left(\frac{r_0^2}{d_0^2} - 2\frac{r_0}{d_0}\sin\theta\right)^p \left(\frac{d_0^2}{(x-x_0)^2 + d_0^2}\right)^{p+\frac{1}{2}} \end{aligned} \quad (2.12)$$

where $C_p = (-1)^p (2p-1)!!/2^p$ are the expansion coefficients for $(1+x)^{-\frac{1}{2}}$ at $x = 0$ and the integer p is chosen large enough to guarantee the accuracy. Then we will have *separable* polynomials instead and the integral (2.7) will be calculated exactly and easily. Finally, the regular integral evaluation boils down to algebraic computations of some pre-computed constants, thus making the calculation free of numerical quadrature and sufficiently efficient. We omit details for brevity. For the other case where $(d_0 + r_0)^2 \ll \min((x_0 - x_1)^2, (x_0 - x_2)^2)$, i.e., the target point is far away along the x-axis direction, similar approximation procedure is also applicable. Similar ideas are applicable to ring element integrals and those in the full-basis method. The approximation method saves computational efforts dramatically. A comparison of the CPU time with and without the Taylor's expansion is given in Table I, and a speed up factor around 50 is observed. The speed up factor increases as the number of wires increases.

TABLE I
COMPARISON OF THE CPU TIME (IN SECONDS) FOR DIRECT AND THE TAYLOR EXPANSION METHOD.

N	171	339	675	1347	2691
Direct	0.830	3.235	12.68	50.76	206.2
Taylor	0.027	0.071	0.270	0.972	3.836

The above comparison infers that there exists some sparsity in the arising matrix, which enable us to use the low rank approximation or tree codes to accelerate the computation, see [11], [12].

III. NUMERICAL RESULTS

Here we present examples to confirm the numerical convergence of the method, and then apply it to both one-wire and multi-wire cases. In all the examples, we set the space charge $\rho = 0$, and so is u_1. With an abuse of notations, we will denote u_2 by u hereafter.

A. Convergence of the method

First, we investigate the convergence using a benchmark with an exact solution. Consider one wire with a radius 0.5 and length 10 in free space, we set the exact solution of u as

$u_{\text{ext}}(\mathbf{x}) = |\mathbf{x}|^{-1}$, and the boundary condition is prescribed as $g(\mathbf{x}) = u_{\text{ext}}\big|_{\Sigma}$ accordingly. Denote the numerical solution by $u^h_{\mathbf{n}} = \partial_{\mathbf{n}} u^{\text{h}}$ and define error function $e^h = \partial_{\mathbf{n}} u_{\text{ext}} - u^h_{\mathbf{n}}$, where $\partial_{\mathbf{n}} u_{\text{ext}}$ is the exact solution of the surface charge density. Fig. 1 shows that the error e^h diminishes uniformly as the mesh size h approaches zero. Therefore, the convergence of the method is clear.

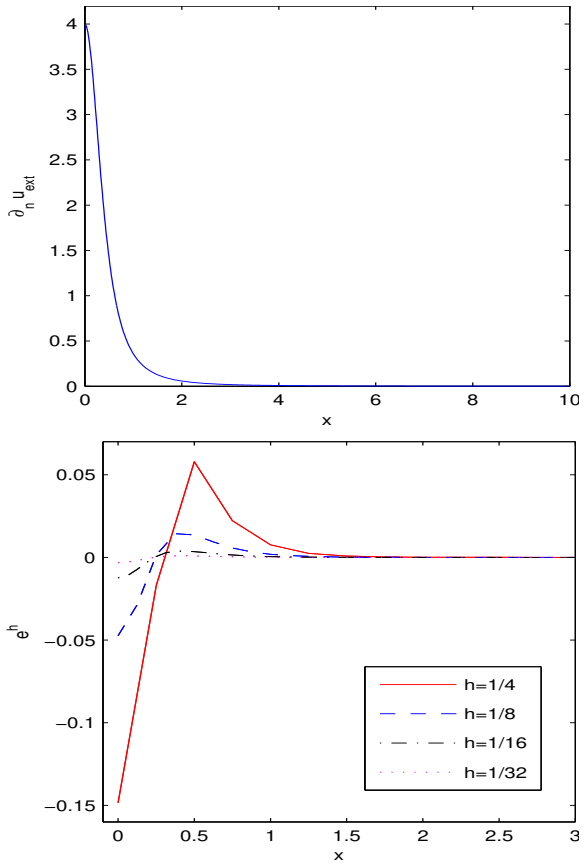

Fig. 1. Exact surface charge density $\partial_{\mathbf{n}} u_{\text{ext}}$ (up); errors e^h with different mesh sizes (down) .

Next, we investigate the convergence for a one-wire case, in which the wire is 20 m long with a radius 2 cm, and is applied a voltage of 50 kV in free space. Fig. 2 plots the electric field $|E|$ on the lateral surface with different mesh sizes versus x-axis near the cylinder end ($x = 10$ m). Numerical convergence is clearly observed.

B. CSM with constant and linear line charge

We also compare the proposed method with CSM. Consider one wire which is 20 m long with a small radius of 2 cm. we place line charges along the x-axis (which is along the conductor) with piecewise constant or linear densities. The target points sit right above the source points. Fig. 3 shows an oscillatory behavior of the calculated piecewise constant line charge Q which is clearly unphysical; while the results by the piecewise linear charge CSM coincide with the scaled density $2\pi r_0 \sigma_h$ computed by the reduced-basis method, and are reasonable.

We clearly see that without a careful treatment of the simulation charges, CSM does not work even for such a simple

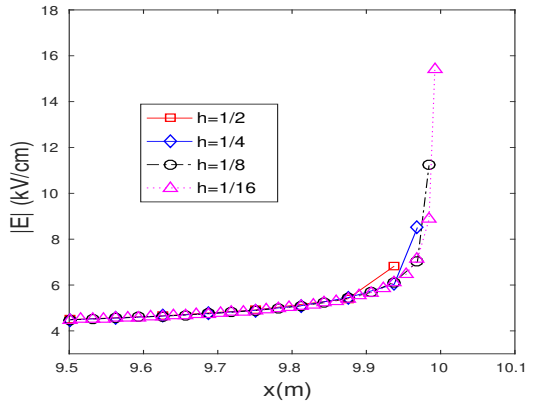

Fig. 2. Convergence test: Electrical field $|E|$ with different meshes.

case, which on the other hand shows the superiority of the BEM.

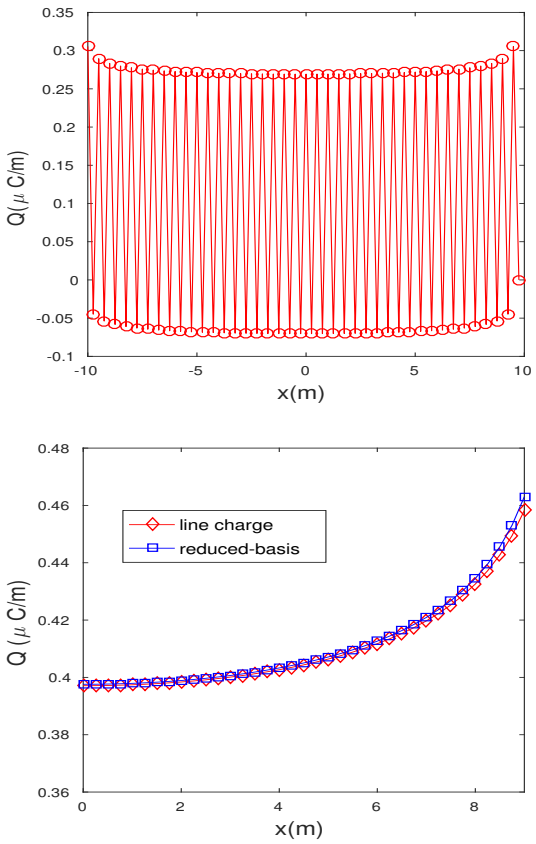

Fig. 3. CSM: Nonphysical oscillatory with piecewise constant line charge (up); Line charge distribution with piecewise linear charge and reduced-basis method (down).

C. The full-basis method and applications

In this example, we assume $\sigma_h \in V_h$ and discretize the azimuth variable uniformly with M points. The density σ_h is piecewise bilinear in x and θ over the cylindrical element, and $M = 4$ by default unless otherwise stated. All the wires are 20 m long, and with a radius of 2 cm, and are with a

voltage of 50 kV. For the cases that consider the influence of the ground plane, the ground plane is considered as a infinite large flat plane with a height of zero (i.e., the x-y plane), and at a zero potential. The ground plane is treated by the well known method of image.

First we consider a one-wire case considering the ground plane, and the wire center is located at $(0, 0, H)^T$. Fig. 4 presents $|E(x, \theta_i)|$ with different heights, where the lines going through $\theta = 0, \pi/2, \pi, 3\pi/2$ are labeled right, up, left and down, respectively. The θ-dependence of the electric field is clearly observed. Compared with the reduce-basis method, the full-basis method would be more accurate considering the ground plane.

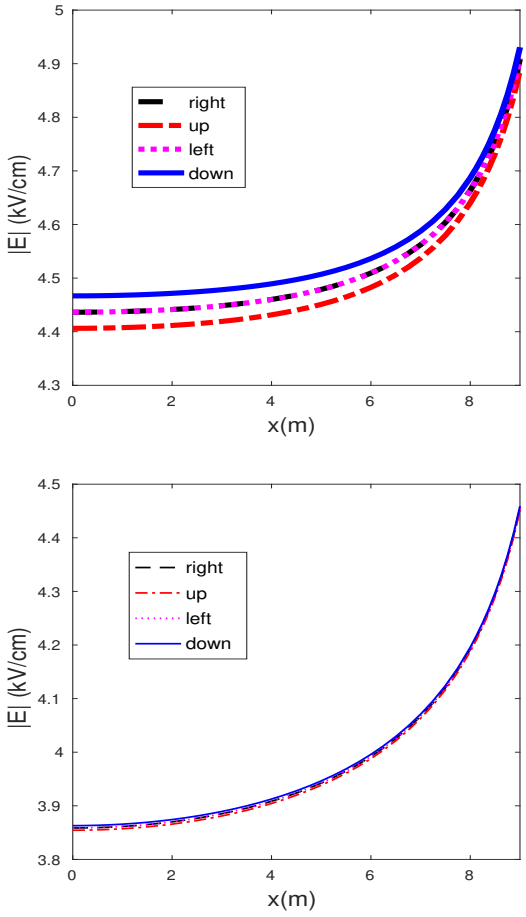

Fig. 4. Electrical field $|E|$ with different height H when the ground plane is present: $H = 3$ (left) and $H = 10$ (right).

Then we investigate the influence of the ground plane by a four-wire case. Assume four wires are centered at $A(0, 10), B(L, 10), C(L, L + 10), D(0, L + 10)$, respectively, i.e., vertexes of a square of length L, in the y-z plane. Here we choose $L = 0.45$ m. Fig. 5 displays the surface electric field $|E|$ of line A accounting for the influence of the ground plane. Besides the θ-dependence of the electric field, we see an increase in $|E|$ (as well as σ_h) when the ground plane is considered.

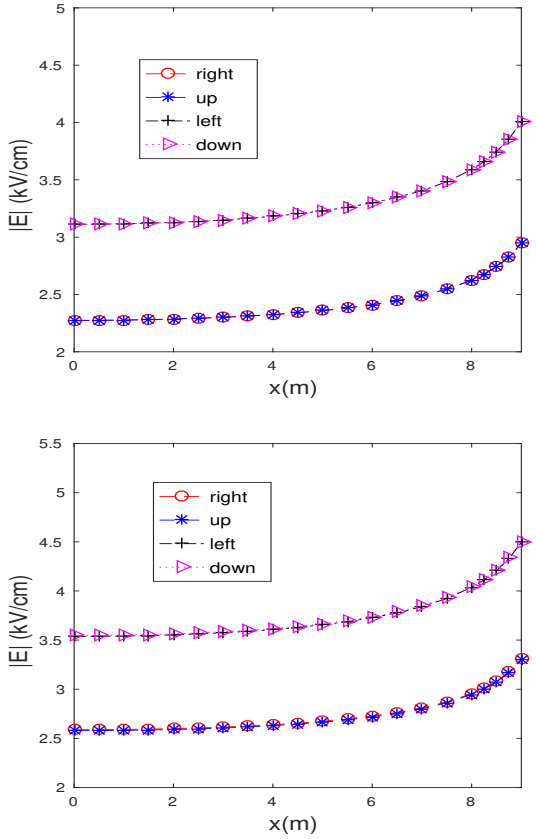

Fig. 5. Electrical field $|E|$ when $H = 10$ m, ground plane missing (up) and present (down).

IV. Conclusions

In this article, we propose a collocation boundary element method, allowing the surface charge density function σ to be either azimuth variable dependent or not.

Detailed numerical quadrature rules are provided for both singular and regular surface integrals. Two common kinds of regular integrals are accelerated greatly by using Taylor's expansion of the distance function when the target point lies far away from the integral element.

Numerical examples are shown to verify the convergence of the method and manifest the potential for the evaluation of electric field around slender conductors.

Acknowledgement

This work was supported by the National Natural Science Foundation of China under grant 51577098, and National key research and development program of China under grant 2016YFB0901005.

References

[1] Rong Zeng, Chijie Zhuang, Xuan Zhou, et al. Survey of recent progress on lightning and lightning protection research. High Voltage. 2016, 1(1): 2-10.

[2] Chijie Zhuang, Hanbo Liu, Rong Zeng and Jinliang He. Adaptive strategies in the leader propagation model for lightning shielding failure evaluation: implementation and applications. IEEE Transactions on Magnetics, 2016, 52(3): 9400604.

[3] Chijie Zhuang, Rong Zeng. A local discontinuous Galerkin method for 1.5-dimensional streamer discharge simulations. Applied Mathematics and Computation. 2013, 219(19): 9925-9934.
[4] Yuesheng Zheng, Bo Zhang, Jinliang He. Onset conditions for positive direct current corona discharges in air under the action of photoionization. Physics of Plasmas, 2011, 18(12):123503.
[5] Zhanqing Yu, Qian Li, Rong Zeng, Jinliang He, Yong Zhang, Zhizhao Li, Chijie Zhuang and Yongli Liao. Calculation of surface electric field on UHV transmission lines under lightning stroke, Electric Power Systems Research, 2013, 94:79-85.
[6] John T. Katsikadelis, Boundary elements: theory and applications, Elsevier Science, 2002.
[7] Y. J. Liu, S. Mukherjee, N. Nishimura, M. Schanz, W. Ye, A. Sutradhar, E. Pan, N. A. Dumont, A. Frangi and A. Saez, "Recent advances and emerging applications of the boundary element method," ASME Applied Mechanics Review, 2011, 64(5):1-38.
[8] S. Mukherjee and Y. J. Liu, "The boundary element method," International Journal of Computational Methods, 2013, 10(6):1350037.
[9] S. Huang and Y. J. Liu, "A new fast direct solver for the boundary element method," Computational Mechanics, 2017,60(3):379-392.
[10] Chijie Zhuang, Yong Zhang, Rong Zeng and Jinliang He. A boundary element method with reduced-basis for computing electric field around Long slim conductors. Proceeding of the IEEE Compumag Conference, Montreal, Canada, 2015.
[11] Chijie Zhuang, Yong Zhang, Xin Zhou, et al. A fast tree algorithm for electric field calculation in streamer discharge simulations. IEEE Transactions on Magnetics. 2018, 54(3): 7201304.
[12] D. Achlioptas and F. McSherry. Fast computing of low rank matrix approximations, Journal of the ACM. 2007,54(2): 9-es.